American Mineralogist, Volume 63, pages 150–159, 1978

Hematolite: a complex dense-packed sheet structure

PAUL B. MOORE AND TAKAHARU ARAKI

Department of the Geophysical Sciences
The University of Chicago, Chicago, Illinois 60637

Abstract

Hematolite, $(Mn^{2+},Mg,Al)_{15}(OH)_{23}(AsO_3)(AsO_4)_2$, $Z = 3$, rhombohedral, space group $R3$, $a = 8.275(5)$, $c = 36.60(5)$A, is a dense-packed oxide structure of unusual complexity. $R = 0.11$ for 1471 independent reflections.

The structure is based on the dense-packed stacking sequence $\cdot hhhch\cdot$ which includes 34 oxygens and one lone electron pair with seven anions per layer. Counting the lone pair as an anion, the general formula is $M_{15}T_3\phi_{35}$, where M = octahedral, T = tetrahedral, and ϕ = anion populations. The arsenite trigonal pyramid is geometrically similar and occurs in an environment similar to that found in synadelphite, $M_9(OH)_9(H_2O)_2(AsO_3)(AsO_4)_2$. The five non-equivalent layers are: (1) isolated octahedra; (2) octahedral and tetrahedral sheet identical to that found in welinite, $Mn^{4+}Mn^{2+}_3SiO_7$; (3) octahedral and trigonal pyramidal sheet much like (2); (4) insular octahedra and tetrahedra, and (5) octahedral sheets of the type $[M_3\phi_7]$ found in chalcophanite. These layers are coupled to each other by corner- and edge-sharing. Hematolite is a key to the more complicated structures of kraisslite, $M^{2+}_{25}Zn_3(OH)_{12}(AsO_4)_4(SiO_4)_8$, and mcgovernite, $M^{2+}_{19}Zn_3(OH)_{21}(AsO_3)(AsO_4)_3(SiO_4)_3$. Models are proposed for these structures and for dixenite, $Mn^{2+}_{11}Mn^{3+}_4(OH)_8(AsO_3)_6(SiO_4)_2$.

Polyhedral averages are $M(1)$–O 2.23, $M(2)$–O 2.22, $M(3)$–O 2.21, $M(4)$–O 2.23, $M(5)$–O 2.04, $M(6)$–O 2.15, $M(7)$–O 2.00, As(1)–O 1.72, As(2)–O 1.79, As(3)–O 1.69 A, with As(2) = As^{3+}. The proposed site distributions are: $M(1) = M(2) = M(3) = M(4) = 1.00\ Mn^{2+}$, $M(5) = 0.44\ Al^{3+} + 0.40\ Mg^{2+} + 0.16\ Mn^{2+}$, $M(6) = 0.56\ Mn^{2+} + 0.44\ Mg^{2+}$, and $M(7) = 0.58\ Al^{3+} + 0.19\ Fe^{3+} + 0.23\ Mn^{2+}$. It is suggested that the ordering scheme optimizes fitting between the sheets.

Introduction

Hematolite, a highly basic arsenite–arsenate of manganese and aluminum, is only known from the Eastern Moss Mine, Nordmark, Värmland, Sweden, where it occurs locally in a basic fissure assemblage associated with calcite, barite, manganosite, pyrochroite, and several other basic manganous arsenates. Our motivation for this study stems partly from its relationship to the other basic arsenate structures shown to be complex articulations of crystallographic dense-packings (Moore, 1967, 1970) and partly because of its relationship with mcgovernite (Wuensch, 1960), a complex species which has the curious property of possessing the largest cell edge yet recorded (other than polytypes) in an inorganic material (204A!).

We shall offer some additional clues to the mcgovernite structure and, with the hematolite structure at hand, feel confident that knowledge of its structure will be "right around the corner."

Experimental details

Owing to the typically bent aspect of hematolite single crystals, difficulty was encountered in obtaining an individual suitable for crystal structure analysis. Our crystal was selected from sample 28939 of the Swedish Natural History Museum, and it is believed that this was one of the specimens which Sjögren (1885) used for his study. The crystal, a flat rhombohedron, measured 0.14 mm along c and 0.25 mm along the a_1- and a_2-axes and could be described satisfactorily by 14 plane faces. A relatively high mosaic spread with an aggregate of multiple splittings for individual reflections required that cell parameters be determined on calibrated precession films (Mo$K\alpha$ radiation) which yielded $a = 8.275(5)$, $c =$

0003-004X/78/0102-0150$02.00

36.60(5)A, space groups $R\bar{3}$ or $R3$. These are in excellent agreement with the results of Berry and Graham (1948).

The crystal was mounted in reverse orientation with its a_2-axis parallel to the rotation axis of a *Pailred* linear diffractometer utilizing graphite-monochromatized Mo$K\alpha$ radiation. Intensities were collected to an upper bound of $2\theta = 60°$ ($\sin\theta/\lambda = 0.70$) and included reciprocal lattice points (hkl) and ($hk\bar{l}$). Owing to high crystal mosaicity, full-peak scan ranges were between 6.4° and 7.8° for automated scans, but a few low-angle and strong reflections required manual scans with somewhat wider angles. Particular care was taken to include, in the integrated intensity, all minor satellite reflections arising from crystal lineage. Scan speeds were 1° min^{-1}, with 20 sec background counts (stationary) on each side of the integrated peak.

Raw intensity data were sorted into three categories. In category (a), the difference in the two background levels was within the expected counting error for a symmetrical peak; in category (b), one background level was more than twice the magnitude of the other and both background levels were significantly higher than the peak profile; (c), values intermediate between (a) and (b). Of the total 1488 I_o's measured, 91 belonged to (b), 389 to (c), and the remainder in (a). For these reflections in (a) and (b) manual scans were made of symmetrical reflections outside the range of the automated region and these were utilized toward final absorption correction. The absorption correction applied the integral method (Burnham, 1966); with transmission-factor ranges from 0.264 to 0.383, this correction was substantial. Symmetry equivalent reflections of the type (000l) were averaged, yielding 1471 independent F_o. Weights assigned to reflections adopted a previously-prescribed procedure (Moore and Araki, 1976a) and included the following errors: long-term fluctuations (0.02), tilting error (0.05°), μ-angle setting error (0.05°), crystal-size error (0.008 mm), ambiguity in linear absorption coefficient (0.25 cm^{-1}), error in numerical integration (0.005), and background-level difference. Indices were transformed to the obverse setting to better facilitate standard description.

Solution and refinement of the structure

An $N(z)$ test in general reflections (Howells *et al.*, 1950) supported a distinctly noncentrosymmetric crystal structure, hence space group $R3$. Patterson synthesis, $P(uvw)$, showed that all vectors had coordinates (u,v) = (0,0), (1/3, 2/3), (2/3, 1/3), (0.31, 0.42), (0.42, 0.11), (0.10, 0.48), (0.48, 0.38), (0.25, 0.20), and (0.05, 0.25). This defines a crystallographic dense-packed system and, with five layers in the asymmetric unit, a problem of considerable difficulty. Hematolite shares the a_1-axis in common with welinite, $Mn^{4+}Mn^{2+}_3SiO_7$, and it was assumed that components of the much simpler welinte structure (Moore, 1968) would also occur in hematolite. One central problem rests on the manner of anion stacking and another problem on the cation-site populations among octahedral and tetrahedral voids in each layer. We employed the formula unit $Mn_{10}Mg_2Al_3(AsO_4)_3(OH)_{24}$, substantiated by the detailed study of Berry and Graham (1948). Successive β-syntheses (Ramachandran and Srinivasan, 1970, p. 96–119), starting with a portion of the structure, eventually led to location of all cations and anions. With 10 nonequivalent cations and 14 nonequivalent cations, least-squares refinement was initiated.

Table 1. Hematolite and dixenite: selected chemical analyses and interpretation

	1	2	3	4	5	6
As_2O_5	21.55	2.82	2.00	-	-	-
SiO_2	-	-	-	5.31	1.65	2.00
As_2O_3	-	-	1.00	32.16	6.07	6.00
Mn_2O_3	-	-	-	8.05	1.90	4.00
Fe_2O_3	1.01	0.19	0.19	3.75	0.88	-
Al_2O_3	6.39	1.89	1.89	-	-	-
MgO	6.66	2.49	2.53	0.32	0.15	-
MnO	49.16	10.43	10.39	43.35	11.40	11.00
CuO	-	-	-	3.49	0.82	-
CaO	0.66	0.18	-	0.39	0.13	-
H_2O	13.93	23.31	23.00	2.80	5.81	8.00
Total	99.36	41.31	41.00	99.91	28.81	31.00

[1]Hematolite. Lundström analysis in Sjögren (1885). MnO = 46.86% and insoluble = 0.64% was reported in that study. MnO = 2.30% was added to the analytical results, assuming the low total was due to an incomplete recovery of this component.

[2]Cations in cell based on sum of cations (other than H) = 18.00.

[3]Computed cation content for $Mn_{10.39}Mg_{2.53}Al_{1.89}Fe^{3+}_{0.19}(OH)_{23}(AsO_3)(AsO_4)_2$. This results from M(1) = M(2) = M(3) = M(4) = Mn^{2+}; M(5) = 0.44 Al^{3+} + 0.40 Mg^{2+} + 0.16 Mn^{2+}; M(6) = 0.56 Mn^{2+} + 0.44 Mg^{2+}; M(7) = 0.58 Al^{3+} + 0.19 Fe^{3+} + 0.23 Mn^{2+}.

[4]Dixenite. Johansson analysis in Wickman (1951). The total includes P_2O_5 = 0.02%, Na_2O = 0.13%, K_2O = 0.14%.

[5]Cations in cell based on sum of cations (other than H) = 23. P^{5+}, Na^+ and K^+ were not included.

[6]Computed cation content for $Mn^{2+}_{11}Mn^{3+}_4(OH)_8(AsO_3)_6(SiO_4)_2$.

Table 2. Hematolite: atomic coordinates and isotropic thermal vibration parameters†

Atom	x	y	z	B(Å²)
M(1)	0	0	0	1.64(7)
M(2)	2/3	1/3	0.2155(2)	1.78(7)
M(3)	0.3124(4)	0.4243(4)	0.0739(1)	1.65(4)
M(4)	0.4111(4)	0.1116(4)	0.1419(1)	1.64(5)
M(5)	0.0935(7)	0.4750(7)	0.2747(2)	1.87(12)
M(6)	0.2503(5)	0.1951(5)	0.2765(2)	1.49(9)
M(7)	0	0	0.0809(2)	1.46(14)
As(1)	0	0	0.1949(1)	1.36(4)
O(1)	0	0	0.2422(5)	1.24(31)
O(3)	0.0590(18)	0.2181(19)	0.1792(4)	1.85(20)
As(2)	1/3	2/3	0.1395(1)	1.38(5)
O(4)	0.1390(18)	0.4986(17)	0.1134(3)	1.43(17)
As(3)	2/3	1/3	0.0608(1)	1.59(5)
O(2)	2/3	1/3	0.1076(5)	0.71(25)
O(5)	0.6003(25)	0.1182(25)	0.0449(5)	3.06(29)
OH(1)	1/3	2/3	0.0454(5)	1.21(28)
OH(2)	1/3	2/3	0.3007(7)	2.41(42)
OH(3)	0.0596(18)	0.2107(20)	0.0468(4)	1.77(20)
OH(4)	0.2252(19)	0.1778(19)	0.1095(4)	1.58(20)
OH(5)	0.6316(18)	0.1180(17)	0.1733(4)	1.84(21)
OH(6)	0.2855(21)	0.4356(21)	0.2474(4)	2.27(26)
OH(7)	0.4171(19)	0.1243(20)	0.2434(4)	1.97(24)
OH(8)	0.0538(18)	0.2465(18)	0.3037(4)	1.80(22)
OH(9)	0.5956(21)	0.0682(20)	0.3088(4)	2.20(23)

†Estimated standard errors refer to the last digit. Site population refinement employed the following scattering curve assignments: M(1) = M(2) = M(3) = M(4) = Mn^{2+}; M(5) = 0.84(3) Al^{3+} + 0.16(3) Fe^{3+}; M(6) = 0.44(3) Al^{3+} + 0.56(3) Mn^{2+}; M(7) = 0.58(4) Al^{3+} + 0.42(4) Fe^{3+}.

We now comment about hematolite's composition. A combination of average polyhedral size, electron density, and site-occupancy refinement for octahedrally coordinated cations afforded an estimate of site distributions. Several analyses for hematolite exist, and the one which best fits our structure study appears in Table 1. At this stage it was clear that the formula unit included two $(AsO_4)^{3-}$ tetrahedra and one $(AsO_3)^{3-}$ trigonal pyramid. The problem then reduced to distributing Mn^{2+}, Fe^{3+}, Mg^{2+}, and Al^{3+} over the octahedral sites. We employed the following scattering curves: Mn^{2+}, Fe^{3+}, and Al^{3+}. The $M(1)$–, $M(2)$–, $M(3)$–, and $M(4)$–O distance averages and electron densities suggested pure Mn^{2+} at these sites. Population refinement on $M(5)$, $M(6)$, and $M(7)$ involved curves for Mn^{2+}, Fe^{3+}, and Al^{3+} and the assumption that these sites are fully occupied. Full-matrix three-dimensional refinement converged to $R = 0.11$ and $R_w = 0.11$ for all 1471 reflections ($R = 0.09$ and $R_w = 0.10$ for 1345 reflections above background) where

$$R = \frac{\Sigma||F_o| - |F_c||}{\Sigma|F_o|} \text{ and } R_w = \left[\frac{\Sigma w(|F_o| - |F_c|)^2}{\Sigma w|F_o|^2}\right]^{1/2}$$

with $w = \sigma^{-2}$ of F_o. Refinement minimized $w(F_o - F_c)^2$. Programs used in this study have been listed earlier (Moore and Araki, 1976a). Scattering curves for Mn^{2+}, Al^{3+}, Fe^{3+}, As^{3+}, As^{5+}, and O^{1-} were obtained from Cromer and Mann (1968) and anomalous dispersion correction, f'', for Mn, Fe, and As from Cromer and Liberman (1970).

Final atomic coordinate and isotropic thermal vibration parameters appear in Table 2. We note that the thermal parameters are about twice those expected for a dense-packed structure, doubtless arising from the inferior quality of the crystal. Since the B's only range from 1.6 to 1.9 A^{-2} for the octahedral cations, the site-population refinement is substantiated. We discuss cation distributions in more detail further on. Table 3 lists the observed and calculated structure factors.[1] The general formula for hematolite is $M_{15}(OH)_{23}(AsO_3)(AsO_4)_2$, with the M cations consisting principally of Mn^{2+} and local solid solution of Mg^{2+} and Al^{3+}.

Topology of the structure

Hematolite is a 15-layer repeat structure along the c-direction with an average separation of 2.44A between layers. Five layers comprise the asymmetric unit and, for full oxygen occupancy, there would be $7 \times 5 = 35$ anion positions. The actual unit formula is $M_{15}(OH)_{23}(AsO_3)(AsO_4)_2$, yielding a total of 34 anions, the one vacancy corresponding to the lone electron pair associated with the $(AsO_3)^{3-}$ trigonal pyra-

Table 4. Cell criteria for hematolite and related compounds

	1	2	3	4	5
a(Å)	8.155(7)	8.275(5)	8.22	8.22(1)	8.22(2)
c(Å)	4.785(5)	36.60(5)	37.44	43.88(5)	203.15(8)
Φ	$P6_3$	R3	R3	$P6_322$	$R\bar{3}c$
N	2	15.(3x5)	15(3x5)	18(3x6)	84(3x28)
D(Å)	2.392	2.439	2.496	2.438	2.418

*Φ is the space group, N the number of dense-packed oxygen layers in the repeat, and D(Å) is the distance between layers.

[1]Welinite. $Mn^{4+}Mn_3^{2+}O_3(SiO_4)$, Z = 2. Data from Moore (1968).

[2]Hematolite. $(Mn^{2+},Mg,Al)_{15}(OH)_{23}(AsO_3)(AsO_4)_2$, Z = 3. This study.

[3]Dixenite. $Mn_{11}^{2+}Mn_4^{3+}(OH)_8(AsO_3)_6(SiO_4)_2$, Z = 3. Data from Wickman (1951).

[4]Kraisslite. $(Mn,Mg)_{25}Zn_3(OH)_{12}(AsO_4)_4(SiO_4)_8$, Z = 2. This study.

[5]McGovernite. $(Mn,Mg)_{19}Zn_3(OH)_{21}(AsO_3)(AsO_4)_3(SiO_4)_3$, Z = 12. Wuensch (1960) and this study.

[1] To obtain a copy of Table 3, order Document AM-78-062 from the Business Office, Mineralogical Society of America, 1909 K Street, N.W., Washington, D.C. 20006. Please remit $1.00 in advance for the microfiche.

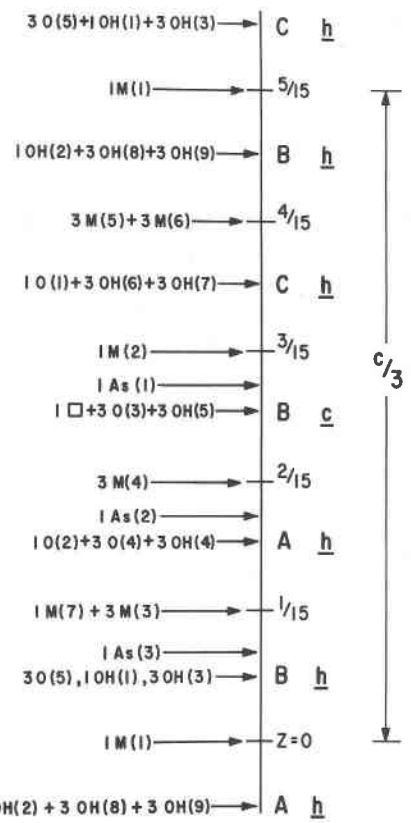

Fig. 1. Stacking sequence for hematolite along the *c*-axis. Heights in *z* are given as fractional coordinates. The layer symbols are given on the right, the distributions of cations and anions on the left. The "" indicates the location of the electron pair associated with As(2).

mid. Thus, hematolite is allied chemically to synadelphite, $M_9(OH)_9(H_2O)_2(AsO_3)(AsO_4)_2$, a mineral which occurs in the same paragenesis (Moore, 1970). Both compounds are based on oxygen dense-packings, but in synadelphite the sequence is $\cdot ch\cdot$ and in hematolite it is $\cdot hhhch\cdot$. In Figure 1, a stacking diagram is shown for hematolite which reveals the distribution of cations and anions and their sequence along the *c*-axial direction. Thus, counting the lone pair as an anion, the general formula for void populations is $M_{15}T_3\phi_{35}$ where M = octahedral populations, T = tetrahedral populations, and ϕ = anion frame. Thus, 3/7 of the available octahedral holes are occupied and 3/70 of the tetrahedral holes are occupied. We compare this with synadelphite, which has $M_9T_3\phi_{24} = M_3T\phi_8$, which leads to 3/8 octahedral and 1/16 tetrahedral occupancies respectively.

In hematolite, the octahedral layers appear at $z = 2m/30$ and the oxygen layers at $(2m + 1)/30$, where m is an integer. The Figure 2 series shows the five distinct layers which comprise hematolite's structural principle. For $m = 0$, 1 $M(1)$ occurs only, and is linked at its corners to octahedra above and below and to 1 $M(7)$ above by a common face. At $m = 1$, 1 $M(7)$ + 3 $M(3)$ + 1 As(3) appear. This arrangement is identical to the sheet noted in the crystal structure of welinite, $M^{4+}M_3^{2+}SiO_7$, which is the simplest repeat $(\cdot h\cdot)$ found among the compounds related by the same a_1-axis (Moore, 1968); at $m = 2$, a similar sheet appears and is comprised of 3 $M(4)$ + As(2), but differs in having no octahedral cation corresponding to $M(7)$ and an $(AsO_3)^{3-}$ trigonal pyramid in place of $(AsO_4)^{3-}$. The $(AsO_3)^{3-}$ trigonal pyramid shares its base with the trigonal array of edges associated with 3 $M(3)$ below, and therefore $(AsO_3)^{3-}$ participates in the same local geometry as found in synadelphite. At $m = 3$, 1 $M(2)$ and 1 As(1) appear. The $M(2)O_6$ octahedron shares its basal edges—3 OH(5)—with the trigonal array of edges associated with 3 $M(4)$ below, and therefore is the region defining the cubic close-packed strip $(\cdot c\cdot)$ in the sequence. Finally, at $m = 4$, the octahedral sheet comprised of 3 $M(5)$ + 3 $M(6)$ occurs. It is, in effect, a pyrochroite sheet with one out of seven octahedra missing, and is identical to the ordering scheme for the $[Mn_3^{4+}O_7]^{2-}$ sheet found in chalcophanite.

Thus, it is seen that hematolite exploits a variety of sheet geometries which doubtless will be shown as similar components in the more complicated structures of kraisslite, $M_{25}^{2+}Zn_3(OH)_{12}(AsO_4)_4(SiO_4)_8$, and mcgovernite, $M_{19}^{2+}Zn_3(OH)_{21}(AsO_3)(AsO_4)_3(SiO_4)_3$, with the welinite-type arrangement as a persistent component in all these structures. With the knowledge of both the synadelphite and hematolite structures at hand, it seems that certain limitations are imposed on local geometry. First, the $(AsO_4)^{3-}$ tetrahedron does not share edges with octahedra in these structures, unlike the edge-sharing (SiO_4) tetrahedra found in welinite, and this probably reflects the greater cation–cation repulsion effect between As^{5+}–M^{2+} compared with Si^{4+}–M^{2+}. Second, the $(AsO_4)^{3-}$ tetrahedron shares its basal oxygens with only one M^{2+} cation and at most two (in synadelphite) and the apical oxygen with three M^{2+} cations. Third, the $(AsO_3)^{3-}$ trigonal pyramid shares its base with a trigonal array of octahedra, suggesting that the $[AsO_3M_3(O,OH)_{10}]$ cluster complex is a locally stable moiety and in fact may be a governing factor in the stabilities of these unusual structures. Fourth, these structures exploit principles of oxygen dense-packing. These observations suggest that the entire problem of investigating these and related structures reduces to

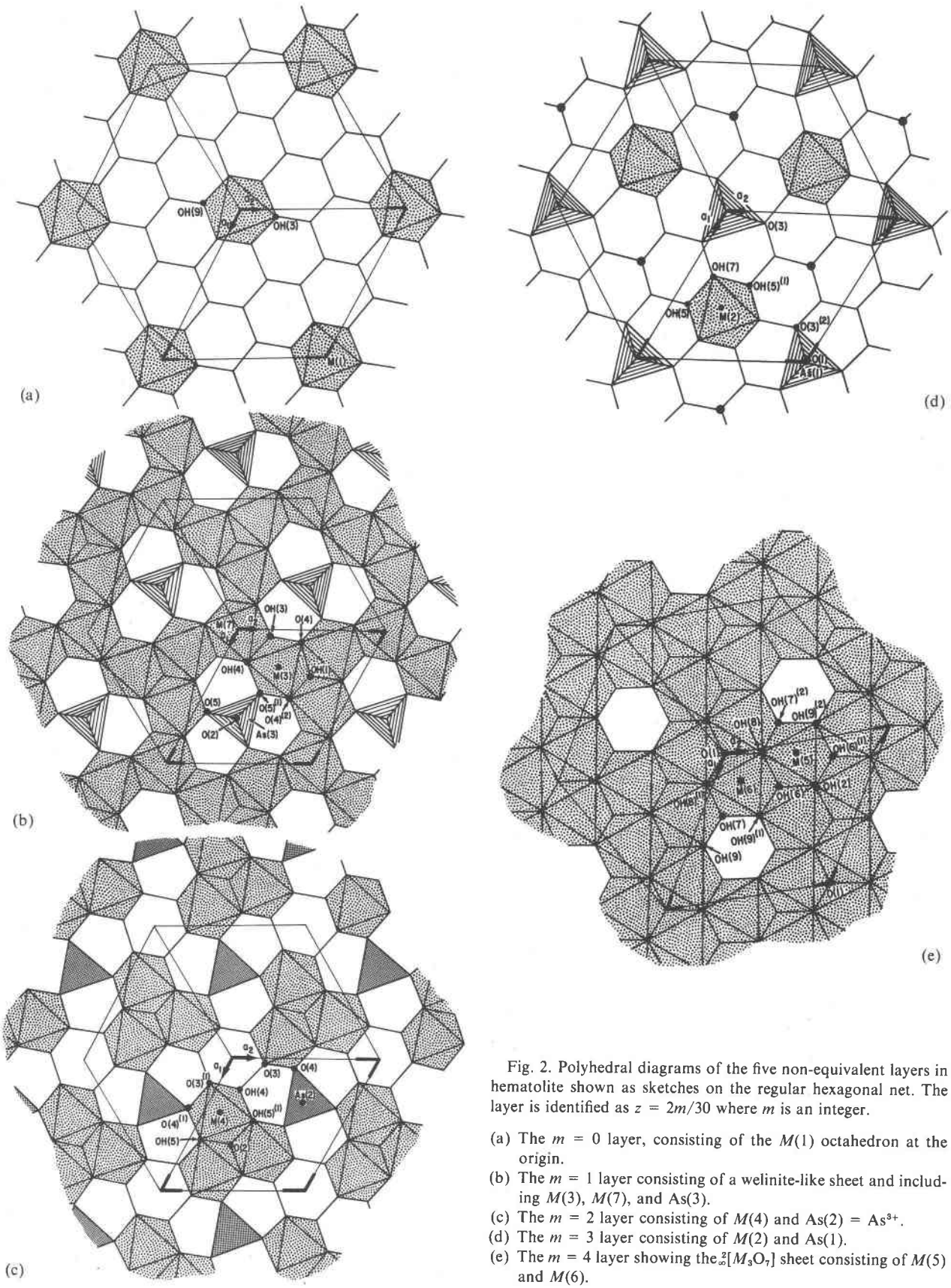

Fig. 2. Polyhedral diagrams of the five non-equivalent layers in hematolite shown as sketches on the regular hexagonal net. The layer is identified as $z = 2m/30$ where m is an integer.

(a) The $m = 0$ layer, consisting of the $M(1)$ octahedron at the origin.
(b) The $m = 1$ layer consisting of a welinite-like sheet and including $M(3)$, $M(7)$, and As(3).
(c) The $m = 2$ layer consisting of $M(4)$ and As(2) = As^{3+}.
(d) The $m = 3$ layer consisting of $M(2)$ and As(1).
(e) The $m = 4$ layer showing the $^{2}_{\infty}[M_3O_7]$ sheet consisting of $M(5)$ and $M(6)$.

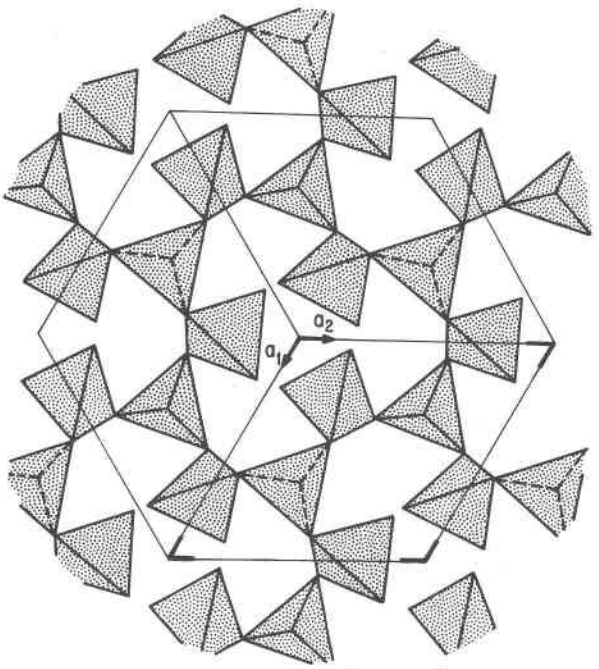

Fig. 3. The $^{2}_{\infty}[Zn_3T_2O_{14}]$ sheet which may occur in the crystal structures of kraisslite and mcgovernite. Note that the ZnO_4 tetrahedra are on 2-fold rotors.

treating the various layers as modular units which, in various combinations, build up an impressive family of structures of seemingly unusual complexity.

Relations to welinite, dixenite, kraisslite and mcgovernite

Table 4 lists the cell relationships among the compounds welinite, hematolite, dixenite, kraisslite,[2] and mcgovernite, cells of which share the $a_1 \sim 8.2$A axis in common. Accepting 2.4A as the layer separation, it is seen that welinite is a 2-layer repeat, hematolite and dixenite are 15-layer repeats, kraisslite an 18-layer, and mcgovernite an 84-layer repeat structure. The last two, however, are by no means as complicated as they seem, for their space groups deem that kraisslite has 5 layers which must be specified in the asymmetric unit, and mcgovernite 8 layers. This is because kraisslite has 2-fold rotors normal to the c-repeat at $z = m/4$, where m is an integer, and mcgovernite has 2-fold rotors at intervals of $z = (2m + 1)/12$. The distinguishing feature of these last two compounds is the presence of both zinc and silicon, suggesting the existence of zincosilicate layers. Recently, the cubic close-packed crystal structure of the paragenetically-related holdenite, $(Mn,Mg)_6Zn_3(OH)_8(AsO_4)_2(SiO_4)$ was found to possess zincosilicate tetrahedral sheets of composition $^{2}_{\infty}[Zn_2SiO_6(OH)_2]$ which link to the octahedral complexes (Moore and Araki, 1977). It is likely, therefore, that these two compounds will be shown to be comprised of layers akin to those found in welinite and hematolite interleaved with zincosilicate or zincoarsenate layers.

A provisional model for these structures is now offered. Symbolize octahedral populations as M and tetrahedral populations as T. One welinite sheet has composition M^{2+}_3T in the xy plane. Call this layer W. In kraisslite the cell has $3 \times 4\ W = 36\ M + 12\ T$. Symbolize the zincosilicate (or zincoarsenate) layer as X. It has composition Zn_3T_2 and the cell has $2\ X = 6$ Zn $+ 4\ T$ (see Fig. 3 for a diagram of its possible arrangement). Call the remaining layer in kraisslite Y. The cell has $4\ Y = 12\ M + 8\ T$ from kraisslite's formula. This $Y = 3\ M + 2\ T$. The proposed sequence is $X(z = 0/18)$–$W(z = 1/18)$–$W(z = 2/18)$–$W(z = 3/18)$–$Y(z = 4/18)$. Now, in mcgovernite a sequence of 5 layers is postulated to be identical to hematolite, giving $M_{15}As^{5+}_2As^{3+}$ in the asymmetric unit. Add an X layer. The remaining two layers are collectively M_4SiAs^{5+}, but it is not possible to suggest their arrangement. The postulated sequence is $X(z = 0/84)$—hematolite (1/84, 2/84, 3/84, 4/84, 5/84)—two unknown layers (6/84, 7/84). Formal crystal-structure analysis, now in progress, will be greatly aided by such an approach, since the homometric character in all these structures is pronounced owing to locally dense-packed sheets.

The Zn_3T_2 postulated layer in Figure 3 is especially appealing, for it is not possible to preserve perfect dense-packing in kraisslite and mcgovernite owing to the presence of the 2-fold rotors. The reason is readily apparent in the cell outline in the xy plane since the a_1- and a_2-axes are not normal to octahedral edges. In the postulated layer, the ZnO_4 tetrahedron is oriented such that its $\bar{4}$-pseudoaxis is parallel to c. On geometrical grounds this is also favored, since the ZnO_4 tetrahedron is substantially larger than either an SiO_4 or AsO_4 tetrahedron and such an orientation leads to a better fitting between adjacent close-packed layers. If such a postulated layer indeed exists, then kraisslite and mcgovernite are in fact *interrupted* dense-packings. It is evident, however, that 2-fold rotors normal to the c-axis exist only in those which contain zinc as a component.

A neat interpretation can be made on the crystal

[2] Kraisslite is a new species recently approved by the International Commission on New Minerals and New Mineral Names. A formal description of this species will appear in a future issue of this journal.

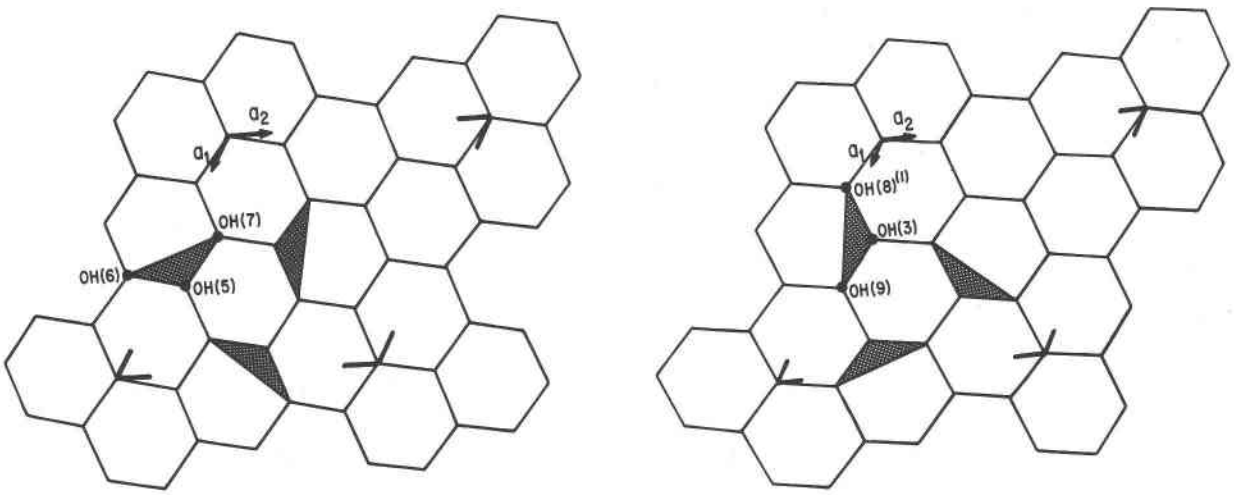

Fig. 4. Proposed distributions of the [AsO_3] trigonal pyramids in the crystal structure of dixenite. These diagrams can be compared with Figs. 2d and 2e.

Table 5. Hematolite: polyhedral interatomic distances and angles

Anions	Coordinating Cations M(1) .333	M(2) .333	M(3) .333	M(4) .333	M(5) .406	M(6) .333	M(7) .462	As(1) 1.250	As(2) 1.000	As(3) 1.250	H_d 0.833	H_a 0.167	Δp_o
O(1)	-----	-----	-----	-----	-----	3	-----	1	-----	-----	-----	-----	+0.25
O(2)	-----	-----	-----	3	-----	-----	-----	-----	-----	1	-----	-----	+0.25
O(3)	-----	-----	-----	1	-----	-----	-----	1	-----	-----		4	+0.25
O(4)	-----	-----	2	1	-----	-----	-----	-----	1	-----	-----	-----	+0.00
O(5)	-----	-----	1	-----	-----	-----	-----	-----	-----	1	-----	3	+0.08
*OH(1)	-----	-----	3	-----	-----	-----	-----	-----	-----	-----	-----	-----	+0.00
*OH(2)	-----	-----	-----	-----	3	-----	-----	-----	-----	-----	-----	-----	+0.22
OH(3)	1	-----	1	-----	-----	-----	1	-----	-----	-----	1	-----	-0.04
OH(4)	-----	-----	1	1	-----	-----	1	-----	-----	-----	1	-----	-0.04
OH(5)	-----	1	-----	2	-----	-----	-----	-----	-----	-----	1	-----	-0.17
OH(6)	-----	-----	-----	-----	2	1	-----	-----	-----	-----	1	-----	-0.02
OH(7)	-----	1	-----	-----	1	1	-----	-----	-----	-----	1	-----	-0.09
OH(8)	-----	-----	-----	-----	1	2	-----	-----	-----	-----	1	-----	-0.09
OH(9)	1	-----	-----	-----	1	1	-----	-----	-----	-----	1	-----	-0.09

Anions	Coordinating Cations, Δd M(1)	M(2)	M(3)	M(4)	M(5)	M(6)	M(7)	As(1)	As(2)	As(3)	Δp_o
O(1)	-----	-----	-----	-----	-----	+0.11(x3)	-----	+0.01	-----	-----	✓
O(2)	-----	-----	-----	+0.12(x3)	-----	-----	-----	----	----	+0.02	✓
O(3)	-----	-----	-----	+0.06	-----	-----	-----	-0.01	-----	-----	✓
O(4)	-----	-----	+0.01,+0.12	-----	-----	-----	-----	-----	+0.00	-----	x
O(5)	-----	-----	-0.11	-----	-----	-----	-----	-----	-----	-0.01	x
OH(1)	-----	-----	-0.02(x3)	-----	-----	-----	-----	-----	-----	-----	✓
OH(2)	-----	-----	-----	-----	+0.01(x3)	-----	-----	-----	-----	-----	x
OH(3)	+0.09	-----	-0.02	-----	-----	-----	+0.00	-----	-----	-----	x
OH(4)	-----	-----	+0.00	-0.01	-----	-----	+0.00	-----	-----	-----	✓
OH(5)	-----	+0.05	-----	-0.10,-0.02	-----	-----	-----	-----	-----	-----	✓
OH(6)	-----	-----	-----	-----	+0.00,+0.01	-0.01	-----	-----	-----	-----	✓
OH(7)	-----	-0.05	-----	-----	-0.01	-0.02	-----	-----	-----	-----	✓
OH(8)	-----	-----	-----	-----	+0.01	-0.03(x2)	-----	-----	-----	-----	✓
OH(9)	-0.07	-----	-----	-----	-0.01	-0.01	-----	-----	-----	-----	✓

†Individual bond strengths are listed under the respective cations and are based on site populations. The deviation from electrostatic neutrality, Δp_o, is given. Deviations in bond distances, Δd, from polyhedral averages are listed. If Δd and Δp_o agree in sign a check is placed, if they do not agree in sign a cross is placed.

Table 6. Hematolite: electrostatic bond strength deviations (Δp_0) and distance deviations (Δd_0)†

M(1)			OH(5)-OH(5)$^{(1)}$	2.87(2)*	82.5(7)
3 M(1)-OH(9)	2.16(1) Å		O(2)-OH(5)	2.92(3)*	81.0(5)
3 M(1)-OH(3)	2.31(1)		O(2)-OH(5)$^{(1)}$	2.92(3)*	79.4(4)
average	2.23 Å		OH(4)-OH(5)$^{(1)}$	3.03(2)	86.4(5)
			O(3)$^{(1)}$-OH(4)	3.10(2)	86.6(5)
3 OH(3)-OH(3)$^{(1)}$	2.70(2)*	71.3(5)°	O(4)$^{(1)}$-OH(5)	3.10(2)	92.3(5)
3 OH(3)-OH(9)$^{(2)}$	3.15(2)	89.6(5)	O(3)$^{(1)}$-O(4)$^{(1)}$	3.18(2)	90.8(5)
3 OH(3)-OH(9)$^{(1)}$	3.18(2)	90.6(5)	O(2)-OH(4)	3.21(1)	89.2(4)
3 OH(9)-OH(9)$^{(1)}$	3.41(2)	104.0(5)	O(3)$^{(1)}$-OH(5)	3.21(2)	101.4(5)
average	3.11	88.9	O(3)$^{(1)}$-OH(5)$^{(2)}$	3.21(2)	90.9(5)
			OH(4)-O(4)$^{(2)}$	3.32(2)	98.7(5)
M(2)			O(2)-O(4)$^{(1)}$	3.44(3)	99.2(4)
3 M(2)-OH(7)	2.17(1)		average	3.13	89.9
3 M(2)-OH(5)	2.27(1)				
average	2.22		**M(5)**		
			M(5)-OH(7)$^{(2)}$	2.03(1)	
3 OH(5)-OH(5)$^{(1)}$	2.87(2)*	78.5(2)	-OH(9)$^{(2)}$	2.03(1)	
3 OH(5)-OH(7)	3.14(2)	89.9(5)	-OH(6)	2.04(1)	
3 OH(5)-OH(7)$^{(2)}$	3.14(2)	89.9(5)	-OH(2)	2.05(1)	
3 OH(7)-OH(7)$^{(1)}$	3.33(2)	99.8(5)	-OH(6)$^{(1)}$	2.05(1)	
average	3.12	89.5	-OH(8)	2.05(1)	
			average	2.04	
M(3)					
M(3)-O(5)$^{(1)}$	2.10(2)		OH(2)-OH(6)$^{(1)}$	2.62(2)*	79.3(6)
-OH(3)	2.19(1)		OH(2)-OH(6)	2.62(2)*	79.7(6)
-OH(1)	2.19(1)		OH(6)-OH(8)	2.72(2)*	83.4(6)
-OH(4)	2.21(1)		OH(7)$^{(2)}$-OH(8)	2.78(2)*	86.2(6)
-O(4)$^{(2)}$	2.22(1)		OH(6)$^{(1)}$-OH(9)$^{(2)}$	2.81(2)*	87.1(6)
-O(4)	2.33(1)		OH(2)-OH(9)$^{(2)}$	2.94(1)	92.1(6)
average	2.21		OH(7)$^{(2)}$-OH(9)$^{(2)}$	2.97(2)	94.0(6)
			OH(8)-OH(9)$^{(2)}$	2.97(2)	93.4(6)
O(4)$^{(2)}$-O(4)	2.62(2)**	70.2(6)	OH(6)-OH(7)$^{(2)}$	2.99(2)	94.5(6)
OH(3)-OH(4)	2.76(2)*	77.5(5)	OH(6)-OH(6)$^{(1)}$	3.03(3)	95.5(8)
O(4)$^{(2)}$-OH(1)	2.91(2)*	82.6(5)	OH(2)-OH(8)	3.07(1)	96.9(6)
O(4)-OH(1)	2.91(2)*	80.3(5)	OH(6)$^{(1)}$-OH(7)$^{(2)}$	3.07(2)	97.6(6)
OH(4)-O(4)	3.08(2)	85.2(5)	average	2.88	90.0
O(5)$^{(1)}$-OH(4)	3.22(2)	96.6(6)			
OH(3)-O(4)	3.24(2)	91.6(5)	**M(6)**		
OH(1)-O(5)$^{(1)}$	3.25(2)	98.8(6)	M(6)-OH(8)	2.12(1)	
O(4)$^{(2)}$-O(5)$^{(1)}$	3.25(2)	97.4(6)	-OH(8)$^{(1)}$	2.12(1)	
OH(1)-OH(3)	3.29(2)	97.5(5)	-OH(7)	2.13(1)	
OH(3)-O(5)$^{(1)}$	3.30(2)	100.8(6)	-OH(6)	2.14(1)	
O(4)$^{(2)}$-OH(4)	3.34(2)	97.5(5)	-OH(9)$^{(1)}$	2.14(1)	
average	3.10	89.7	-O(1)	2.26(1)	
			average	2.15	
M(4)					
M(4)-OH(5)	2.13(1)		OH(6)-OH(8)	2.72(2)*	79.0(6)
-O(4)$^{(1)}$	2.16(1)		OH(7)-OH(8)$^{(1)}$	2.78(2)*	82.0(6)
-OH(5)$^{(1)}$	2.21(1)		OH(6)-OH(9)$^{(1)}$	2.81(2)*	82.0(6)
-OH(4)	2.22(1)		O(1)-OH(8)$^{(1)}$	2.92(2)*	83.5(4)
-O(3)$^{(1)}$	2.29(1)		O(1)-OH(8)	2.92(2)*	83.3(4)
-O(2)	2.35(1)		OH(8)-OH(9)$^{(1)}$	3.04(2)	90.7(5)
average	2.23		O(1)-OH(7)	3.07(1)	88.7(5)
			O(1)-OH(6)	3.18(2)	92.2(5)
			OH(7)-OH(9)$^{(1)}$	3.20(2)	97.1(5)
			OH(8)-OH(8)$^{(1)}$	3.22(2)	98.7(7)
			OH(6)-OH(7)	3.26(2)	99.6(6)
			OH(8)$^{(1)}$-OH(9)$^{(1)}$	3.32(2)	102.2(6)
			average	3.04	89.9

M(7)				
3 M(7)-OH(3)	2.00(1)			
3 M(7)-OH(4)	2.00(1)			
average	2.00			
3 OH(3)-OH(3)$^{(1)}$	2.70(2)*	85.0(6)		
3 OH(3)-OH(4)	2.76(2)*	87.3(6)		
3 OH(3)-OH(4)$^{(2)}$	2.88(2)	92.4(5)		
3 OH(4)-OH(4)$^{(1)}$	2.95(2)	95.1(9)		
average	2.82	90.0		
As(1)				
3 As(1)-O(3)	1.71(1)			
1 As(1)-O(1)	1.73(2)			
average	1.72			
3 O(3)-O(3)$^{(1)}$	2.80(2)	109.4(4)		
3 O(1)-O(3)	2.82(2)	109.6(4)		
average	2.81	109.5		
As(2)				Syna
3 As(2)-O(4)	1.79(1)			
average	1.79		1.76	
3 O(4)-O(4)$^{(1)}$	2.62(2)**	94.2(5)		
average	2.62	94.2	2.61	95.7
As(3)				
3 As(3)-O(5)	1.68(2)			
1 As(3)-O(2)	1.71(2)			
average	1.69			
3 O(5)-O(5)$^{(1)}$	2.73(3)	108.7(6)		
3 O(2)-O(5)	2.79(2)	110.3(6)		
average	2.76	109.5		
Hydrogen Bonds				
OH(4)···O(3)	2.99(2)			
OH(5)$^{(1)}$···O(3)	3.11(2)			
OH(6)···O(3)	3.10(2)			
OH(7)$^{(2)}$···O(3)	3.02(2)			
OH(3)$^{(1)}$···O(5)	3.24(2)			
OH(8)···O(5)	3.23(2)			
OH(9)$^{(1)}$···O(5)	3.19(2)			

*O–O′ shared edges between octahedra, **O–O′ shared edges between octahedron and As(2)O_3 trigonal pyramid. (1) = y-x, -x, z; (2) = -y, x-y, z applied to atom coordinates in Table 2.

chemistry of dixenite. This phase is structurally related to hematolite, as pointed out by Wickman (1951), and is clearly seen in the cell relationships in Table 4. We suspect that dixenite is in fact a "stuffed" derivative structure of hematolite, and we propose a structure model for it. Remove As(2)(= As^{3+}) and replace O(4) by $(OH)^-$. Replace OH(3), OH(8), and OH(9) by *oxo*-anions coordinated to As^{3+}. The trigonal pyramid thus produced shares edges with *M*(1)–O and *M*(5)–O octahedra. Replace OH(5), OH(6), and OH(7) by *oxo*-anions, also coordinated to As^{3+}. Its trigonal pyramid shares edges with *M*(2)–O and *M*(5)–O octahedra. Finally, replace As(1) and As(3)(=As^{5+}) by Si^{4+}. The resulting end-member composition is $Mn^{2+}_{11}Mn^{3+}_4(OH)_8(AsO_3)_6(SiO_4)_2$, and agrees well with the dixenite analysis in Table 1 if a

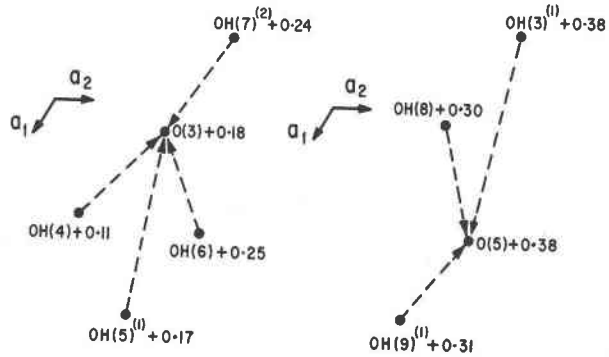

Fig. 5. Arrangements of hydrogen bonds suggested for the crystal structure of hematolite. Heights are given as fractional coordinates in z.

slightly greater oxidation grade is assumed. Like hematolite and synadelphite, the (AsO_3) trigonal pyramids share edges with octahedra, but unlike these minerals the pyramids are *canted* and not normal to the c-axial direction (Fig. 4). This model conserves isomorphism of the oxygen framework in the two structures (including the void) and isomorphism among the populated octahedral and tetrahedral sites. In dixenite, the As^{3+} cations are situated in the relatively open layers of the structure, at $z \sim 0$ and 3/15, according to this model.

Polyhedral interatomic distances and angles

Table 5 summarizes the polyhedral interatomic distances and angles found for our hematolite crystal. The $M(1)$–, $M(2)$–, $M(3)$–, and M(4)–O distances correspond to those for essentially pure Mn^{2+}–O distances and confirm the condition of refinement in Table 2. $M(5)$, $M(6)$, and $M(7)$ must involve mixed cations, and since it is not possible to discriminate Mg^{2+} and Al^{3+}, and Mn^{2+} and Fe^{3+} in the refinement, we are forced to propose site populations which best fit the refinement, the chemical analysis, and the bond-distance averages. We propose $M(5)$ = 0.44 Al^{3+} + 0.40 Mg^{2+} + 0.16 Mn^{2+}; $M(6)$ = 0.56 Mn^{2+} + 0.44 Mg^{2+}; and $M(7)$ = 0.58 Al^{3+} + 0.19 Fe^{3+} + 0.23 Mn^{2+}. The mean M–O distances [compared with the computed values in parentheses obtained from the tables of Shannon and Prewitt (1969)] are: $M(5)$–O = 2.04(2.06), $M(6)$–O = 2.15(2.17), and $M(7)$–O = 2.00(2.02)A. The $M(7)$–O octahedron is the smallest of the seven nonequivalent octahedra and accommodates predominately M^{3+} cations. This is entirely consistent with the $M(1)$–O octahedron in welinite (Moore, 1968), which accommodates octahedral cations of higher charge (mainly Mn^{4+}) and which plays a structurally similar role. The site distributions doubtless optimize fitting of the successive sheets in the asymmetric unit in much the same way that mixed cation distributions optimize fitting between dissimilar chains in the "3A wallpaper structures" (Moore and Araki, 1974). Thus, it is likely that hematolite cannot exist as a pure end-member but requires extra components (Mg^{2+}, Al^{3+}, and Fe^{3+}) for its stabilization.

Table 5 also reveals that the $(AsO_3)^{3-}$ trigonal pyramids in hematolite and synadelphite are of similar geometry and that the O–As–O′ angle is in the range 95 ± 1°. This is significantly more acute than the O–T–O′ angles found in silicates where edges are shared, and appears to be a geometrical property characteristic of the $(AsO_3)^{3-}$ trigonal pyramid. Moore and Araki (1976b) have discussed the analogous $(SbO_3)^{3-}$ trigonal pyramid in considerable detail and found an O–Sb–O′ angle 92.1° in derbylite. Ranges of O–Sb–O′ from 79.8° to 98.1° have been found in valentinite (Svensson, 1974).

Without exception, the shared edges are the shortest distances among their polyhedra. Finally, bond length–bond strength assignments were made (Table 6), using the procedure of Baur (1970). Owing to dense-packing, assignment of hydrogen bonds is not simple and the results must be treated with caution. Seven nonequivalent bonds are proposed, with O(3) accepting four bonds and O(5) accepting three. The local configurations are shown in Figure 5. O(3) almost certainly accepts at least three bonds, since its distance average to the coordinating cations is longer than the polyhedral averages. In the absence of H-bonds, this anion would be severely undersaturated with $\Delta p_0 = -0.47$. The assignment of three H-bonds to O(5) is less certain, since the average distances are shorter than the polyhedral averages. On the other hand, the O · · · O(5) distances are rather long (3.19 to 3.24A), suggesting weak bonds. Assignment of H-bonds arising from OH(1) and OH(2) are uncertain, but their contribution would be weak since the H-atoms would be oriented along trigonal axes and contribute only $x = 1/3 \times 1/6 = 1/18$ in average bond strength.

Acknowledgments

We are grateful to the National Science Foundation which supported this study through the EAR75-19483 (Geochemistry) grant and through the Materials Research Laboratory grant awarded to The University of Chicago. We also appreciate loan of the sample from the Swedish Natural History Museum, in particular to Dr. Eric Welin who made the arrangement possible.

References

Baur, W. H. (1970) Bond length variation and distorted coordination polyhedra in inorganic crystals. *Trans. Am. Crystallogr. Assoc.*, *6*, 129–155.

Berry, L. G. and A. R. Graham (1948) X-ray measurements on brackebuschite and hematolite. *Am. Mineral.*, *33*, 489–495.

Burnham, C. W. (1966) Computation of absorption corrections, and the significance of the end effect. *Am. Mineral.*, *51*, 159–167.

Cromer, D. T. and D. Liberman (1970) Relativistic calculation of anomalous scattering factors for X-rays. *Los Alamos Scientific Laboratory, Univ. of Calif. Rep. LA-4403, UC-34.*

——— and J. B. Mann (1968) X-ray scattering factors computed from numerical Hartree-Fock wave-functions. *Acta Crystallogr.*, *A24*, 321–324.

Howells, E. R., D. C. Phillips and D. Rogers (1950) The probability distribution of X-ray intensity. II. Experimental investigation on the X-ray detection of center of symmetry. *Acta Crystallogr.*, *3*, 210–214.

Moore, P. B. (1967) Crystal chemistry of the basic manganese arsenate minerals. I. The crystal structures of flinkite and retzian. *Am. Mineral.*, *52*, 1603–1613.

——— (1968) The crystal structure of welinite. *Ark. Mineral. Geol.*, *4*, 459–466.

——— (1970) Crystal chemistry of the basic manganese arsenates. IV. Mixed arsenic valences in the crystal structure of synadelphite. *Am. Mineral.*, *55*, 2023–2037.

Moore, P. B. and T. Araki (1974) Pinakiolite, warwickite and wightmanite: Crystal chemistry of complex 3A wallpaper structures. *Am. Mineral.*, *59*, 985–1004.

——— (1976a) A mixed-valence solid-solution series: crystal structures of phosphoferrite and kryzhanovskite. *Inorg. Chem.*, *15*, 316–321.

——— (1976b) Derbylite, a novel close-packed oxide structure. *Neues Jahrb. Mineral. Abh.*, *126*, 292–303.

——— (1977) Holdenite, a novel cubic close-packed structure. *Am. Mineral.*, *62*, 513–521.

Ramachandran, G. N. and R. Srinivasan (1970) *Fourier Methods in Crystallography.* Wiley-Interscience, New York.

Shannon, R. D. and C. T. Prewitt (1969) Effective ionic radii in oxides and fluorides. *Acta Crystallogr.*, *B25*, 925–946.

Sjögren, Hj. (1885) IX. Ueber die Manganarseniate von Nordmarken in Wermland. *Z. Krystallogr.*, *10*, 115–155.

Svensson, Ch. (1974) The crystal structure of orthorhombic antimony trioxide. *Acta Crystallogr.*, *B30*, 458–461.

Wickman, F. E. (1951) From the notes of the late K. Johansson. VII. A revised chemical analysis of dixenite from Långban. *Geol. Fören. Förhandl.*, *73*, 637–638.

Wuensch, B. J. (1960) The crystallography of mcgovernite, a complex arsenosilicate. *Am. Mineral.*, *45*, 937–945.

Manuscript received, March 25, 1977; accepted for publication, August 15, 1977.